ORIGINAL PAPER

An analysis of global ionospheric disturbances and scintillations during the strong magnetic storm in September 2017

Xin Song[1] · Rong Yang[1] · Xingqun Zhan[1]

Abstract

Severe space weather events, e.g., solar flares and magnetic storm, can cause significant disturbances to the global ionosphere. The radio frequency signals, such as wireless communications and global satellite navigation system (GNSS) signals, often experience strong scintillations when traveling through the disturbed ionosphere layer. On 6 September 2017, the sun emitted the largest solar flare classified X9.3 since the 24th solar activity week. It triggered the geomagnetic storm and ionospheric storm on September 8, causing severe disturbances and scintillations of ionospheric. In this work, we take this event as the objective to investigate the characteristics of the ionosphere disturbance. First, the temporal and spatial distributions of ionospheric total electron content (TEC) are analyzed using the ground-based IGS data. The change of TEC is highly correlated with that of the geomagnetic indices and the magnetic storm has the greatest impact on low latitudes. Then, a five-point moving average method is adopted to extract the spatial fluctuations based on post-processed electron density and TEC data from COSMIC and GRACE missions. We find they show different disturbance characteristics in spatial distribution. In addition, the GNSS amplitude scintillation index S4 which is available from the COSMIC satellite mission is used to characterize ionospheric scintillation during this event. Weak scintillation occurred in most parts of the world on September 8 2017, while moderate scintillation is mainly concentrated around 120° W and 100° E. Our study can provide a basis for better evaluating the impact of ionosphere disturbance changes on satellite communication and navigation in space weather events.

Keywords TEC · Ionospheric disturbances · Magnetic storm event · Ionospheric scintillations

1 Introduction

The ionosphere refers to the upper atmosphere at a distance of 60–1000 km from the surface of the earth, which is defined by the International Association of Radio Engineers (IRE) as an area where "there are enough free electrons that can significantly affect radio wave propagation". The Total Electron Content (TEC) and electron density of the ionosphere are important parameters to characterize the ionosphere, which have different temporal and spatial distributions, especially during geomagnetic storms [1]. According to the maximum distribution of electron density with height, the ionosphere is divided into D, E, F layers, and the topside ionosphere [2]. The F layer can be divided into F1 and F2 layers in the day-time and the F1 layer disappears at night. The electron density of the F layer is much higher than that of the D layer and the E layer, and it has the strongest reflection on radio waves. The F layer is typically used in the long-distance communication system which can reflect the High-Frequency (HF) signals.

The ionosphere absorbs solar energy to maintain the complex energy exchange and dynamic balance. However, the balance will be broken in the presence of the space weather event. For example, during a solar storm, the sun releases high-energy protons and electrons and intense radiation in all wavelengths [3]. Then, a large number of strong ultraviolet radiation injects into the ionosphere, which will enhance the ionospheric electron density, thereby increasing the atmospheric resistance suffered by the spacecraft and decreasing the orbital altitude. And these high-energy charged particles can directly interact with the electronic devices and materials on the spacecraft and cause direct damage to the spacecraft. Moreover, it will produce a large number of ionospheric

✉ Xingqun Zhan
  xqzhan@sjtu.edu.cn

[1] School of Aeronautics and Astronautics, Shanghai Jiao Tong University, Shanghai 200240, China

irregularities, and induce ionospheric scintillation to the radio signals.

More specifically, the ionospheric scintillation refers to a phenomenon of rapid fluctuations on the signal amplitude and phase due to the presence of random electron density irregularities when radio waves pass through the ionosphere. The most likely areas to have ionospheric scintillation occurrences are the low latitude areas locating within $\pm 20°$ of the magnetic equator and the polar regions. During the strong ionospheric scintillations, the signal interruption will cause cycle slips or even complete loss of lock in GNSS receivers [4]. Yang [5] investigated the equatorial ionospheric scintillation using GNSS observations from Hong Kong during the 24th solar cycle and provided a study of temporal–spatial characteristics of ionospheric scintillations as well as the variability of ionospheric plasma irregularities associated with scintillation, which occur frequently during active solar activities.

In September 2017, the sunspot group AR2673 became active that triggered a series of solar flare events and brought a large number of high-energy charged particles and plasma clouds, as well as sharply enhanced electromagnetic radiation. Especially at UTC 11: 53 on September 6 [6], the strongest flare at the magnitude of X9.3 within the 24th solar cycle had broken out, the accompanying coronal mass ejection (CME) reached the earth after rapid propagation of 31 h, triggering the geomagnetic storm and ionospheric storm on September 8, causing severe ionospheric disturbances and scintillations in the worldwide.

Yasyukevich et al. [3] studied the effects of the X2.2 and X9.3 solar flares of 6 September 2017 on the Earth's ionosphere, GNSS-based navigation, and HF-radio propagation. They found that the $X2.2$ solar flare had caused an overall increase of 2–4 TECU on the dayside, the X9.3 solar flare had produced a sudden increase of 8–10TECU at midlatitudes and of 15–16 TECU enhancement at low latitudes in the ionospheric absolute vertical total electron content. Lei et al. [7] have investigated the ionospheric responses in the Asian–Australian sector during the September 2017 geomagnetic storm based on the Beidou geostationary orbit satellites observations. They found long-duration daytime TEC enhancements even during the storm recovery phase from 7 to 12 September 2017. Hocke et al. [8] extracted the fluctuations in electron density and TEC using high-pass filtering in the s domain (the distance between a reference point and the tangent point) based on reprocessed profiles of electron density and TEC from the COSMIC mission. They found that the TEC at solar maximum (September 2013) had stronger fluctuations than those at solar minimum (September 2008).

Our study aims at the investigation of the ionospheric responses to the magnetic storm in September 2017. First, the temporal and spatial distributions of ionospheric TEC during

the geomagnetic storm are analyzed using the ground-based IGS data. Then, the spatial fluctuations based on post-processed electron density and TEC are extracted referring to the study of Hocke et al. [8], but, differently, we apply a five-point moving average method to extract the low-frequency component as the smoothed value. The disturbance value, which is the extracted high-frequency component, is the difference between the original value and the smoothed value. After extracting the fluctuations, different standards are adopted to count the fluctuations of electron density and TEC. And due to the sparse data of single satellite mission, the space-based radio occultation data from COSMIC and GRACE missions are fused to make the data dense. Finally, the global distribution of ionospheric scintillation index $S4$ during magnetic storms is given, which is defined as a random modulation of signals when propagating through ionospheric irregularities [9].

There have been many studies to examine the effects of electric fields, thermospheric dynamics, and neutral composition changes on ionospheric variations during storms using TEC data from various sources [7]. Our goal is to analyze the disturbance characteristics of the ionosphere at different latitudes and longitudes in this event using ground-based and space-based data. On the one hand, our analysis is helpful to reveal the physical mechanism of the ionospheric disturbances, which can interfere with the satellite navigation and communication systems, e.g., the Global Navigation Satellite System (GNSS) [10]. On the other hand, ionospheric delay correction is a key factor to improve the accuracy of GNSS positioning, and TEC is closely related to the time delay of ionospheric radio wave propagation, so it can be used for radio wave propagation correction in satellite positioning and navigation. Moreover, our analysis method is also applicable to other space weather/magnetic storm events.

The organization of the paper is as follows. Section 2 describes the geomagnetic storms and data processing for the extraction of ionospheric fluctuations. The results and analysis are shown and discussed in Sect. 3.

2 Data and method

2.1 Geomagnetic data

Geomagnetic storm is a strong disturbance of the earth's magnetic field. The interplanetary 3-h magnetic index (Kp) describes the intensity of the earth's magnetic field disturbance during the 3 h. The Kp index is divided into ten levels from 0 to 9. The larger the number, the greater the disturbance amplitude. Generally speaking, Kp = 4 or 5 represents small magnetic storm, and Kp≥ 7 represents large magnetic storm (http://www.sepc.ac.cn). In the histogram, we use the green column to indicate the geomagnetic calm, and the red column

to indicate the geomagnetic storm. During a magnetic storm, the disturbance of the magnetic field is mainly caused by the equatorial ring current. Therefore, the magnetic storm ring current index (Dst) is introduced, and the unit is nanotesla (nT). Dst index is one value per hour, which can more accurately reflect the geomagnetic disturbance. In this study, we used Kp and Dst indices provided by the Space Environment Prediction Center (SEPC) of the Center for Space Science and Applied Research, Chinese Academy of Sciences (http://www.sepc.ac.cn/tecchn.php) as auxiliary data.

2.2 Ground-based data

To understand the effects of the September 2017 geomagnetic storm on the ionosphere, it is of interest to first estimate their global distribution. For this purpose, we analyze the global ionospheric total electron content map. The Ground-based data used in this study are acquired from the Ionosphere Monitoring and Prediction Center organized by the International GNSS Service (IGS). The IGS Global Ionospheric Map (GIM) of vertical TEC (VTEC) is in Ionosphere map Exchange (IONEX) format [11], which are accessible at ftp://cddis.gsfc.nasa.gov/pub/gps/products/ionex. The GIM is generated routinely by the IGS community with a spatial resolution of $5° \times 2.5°$ (longitude × latitude) and a temporal interval of 2 h [12]. The Kp and Dst indices characterize the intensity of geomagnetic disturbance. Associating the changes of the Kp index and Dst index, we can analyze the temporal and spatial response of global Ionospheric TEC to the geomagnetic storm.

2.3 Space-based data

The space-based data are obtained from COSMIC Data Analysis and Archive Center (CDAAC, http://cdaac-www.cosmic.ucar.edu/cdaac/products.html). The post-processed electron density Ne and TEC profiles from COSMIC (Constellation Observing System for Meteorology, Ionosphere, and Climate) and GRACE (Gravity Recovery And Climate Experiment) missions are obtained from "ionPrf" files and the S4 data are obtained from COSMIC "scnLv1" file.

The COSMIC is a joint scientific mission of Chinese Taiwan and the USA consisting of six low earth orbiting (LEO) microsatellites [13]. It can monitor Earth's atmosphere with unprecedented long-term stability, resolution, coverage, and accuracy [14]. A detailed description of the COSMIC mission can be found in Anthes et al. [15]. COSMIC could provide up 1500–2500 decent soundings of the ionosphere and atmosphere per day at the early stages of its operation, but due to the aging and loss of the satellites, the number of profiles declined severely after 2014 [16]. As a result, in September 2017, we only have about 150 profiles per day.

The GRACE satellites are in a near-circular, near-polar orbit since the first launch on 17 March 2002 with an initial altitude of 500 km. However, the natural decay of the orbital altitude since launch is about 1.1 km/month [17]. Therefore, as of September 2017, it is found that the highest orbit height detected by GRACE RO measurement is about 350 km, at the peak height of F2 layer.

Lei et al. [18] compared the electron densities retrieved from the COSMIC RO measurements with incoherent scatter radars and ionosondes. The results showed the Electron Density Profiles (EDPs) of COSMIC are in agreement with another two measurements. Zakharenkova et al. [12] analyzed and tested the validity of COSMIC data by comparison with ionosondes and IGS data. They found there was good consistency between them and the most pronounced effect of the electron density increase occurred at the altitude range of 300–350 km. Therefore, we combined the RO data of COSMIC and GRACE to analyze the global distribution of Ne and TEC disturbance of 300–350 km on September 8, 2017.

2.4 Data processing

GPS radio occultation can be regarded as a bistatic limb sounding of the atmosphere where the transmitter is on a GPS satellite and the receiver is on a low Earth orbit (LEO) satellite [8]. At CDAAC, the ionospheric profiles are retrieved by the Abel inversion from TEC along LEO-GPS rays. The Ne is assumed to be local spherical symmetric. This assumption may introduce systematic errors. Also, the Ne profile is a curve, not a straight line, which means there are horizontal and time fluctuations in the presence of ionospheric irregularities. But in this study, we only focus on its vertical changes and ignore the horizontal and temporal fluctuations. More details about electron density inversion can be found in Kuo et al. [19] and Syndergaard et al. [20]. It should be noted that the TEC profile in "ionprf" is the calibrated TEC which is calculated by subtracting the measurements at positive elevation angles from those at negative elevation angles [18].

Besides, due to the influences of observation errors (e.g., cycle slips in GPS phase data) and the approximations used in the inversion process, some profiles may have gross errors. Therefore, a quality control approach to remove unreasonable profiles is necessary. In this study, the qualities of profiles are checked using the criteria applied in the references [21–23]. (1) According to the statistics of the peak height of F2 layer during high solar activity by Sun [24], the profiles with peak height hmF2 550 km beyond or 180 km below are removed; (2) the profiles with peak electron density NmF2 greater than $10^7 el/cm^2$ are removed; (3) the profiles without significant peak electron density are removed. For

this purpose, two slopes (Slope1, Slope2) are defined to filter the data as follows:

$$Slope1 = \frac{Ne(h_2) - Ne(h_{max})}{h_2 - h_{max}}, \qquad (1)$$

$$Slope2 = \frac{Ne(h_{max}) - Ne(h_1)}{h_{max} - h_1}, \qquad (2)$$

where h_2 represents the maximum height corresponding to a single electron density profile data within the height range of 150–450 km from the ground, $Ne(h_2)$ is the electronic density value at the height of h_2. h_1 represents the minimum height corresponding to the single electron density profile data within the height range of 150–450 km from the ground, and Ne (h_1) is the electronic density value at the height of h_1. Ne (h_{max}) and h_{max} represent the peak electron density of F2 layer and its corresponding height. According to the above criterion, the profiles with Slope1 > 0 or Slope2 < 0.1 are removed.

We extract the fluctuations in Ne and TEC profiles by a five-point moving average process. Figure 1a shows an example of disturbed electron density profile Ne (blue line) and the corresponding smoothed values Ne' (red line) at 52 ° N, 158 ° E during the geomagnetic storm of 8 September 2017. Panel (b) shows the electron density fluctuations Ne[*] filtered by five-point moving average method. Then, we carry out a similar analysis for TEC profiles of the same occultation event in Fig. 1c, d. We find that for Ne, the GRACE satellite and COSMIC show a good consistency in using percentage, that is, the smoothed value minus the observed value, then divided by the smoothed value and finally take the absolute values, which represents the amplitude of Ne fluctuation. But for TEC, the GRACE satellite and COSMIC show a good consistency in using the root mean square (RMS) of these two sequences. So for each fluctuation profile, we calculate the mean of the percentage of fluctuations for electron density and the RMS of the fluctuations for TEC within the altitude range 300–350 km, which is defined as ΔNe or ΔTEC, respectively. The ΔNe and ΔTEC values of the selected profiles are binned into 10° × 10° (latitude × longitude) grid cells referring to [8] and take the maximum value in each grid to get the global distribution of F2 peak region disturbance.

For the S4 index, we calculate the tangent coordinates of each occultation ray, which means the tangent height is between 80 and 800 km and the LEO satellite is at a negative elevation angle. Then we divided the global map into 19 × 37 (latitude × longitude) grids and marked S4 with longitude and latitude coordinates of tangent points.

3 Results and analysis

3.1 Results from ground-based data

Figure 2 presents the variations of geomagnetic activity indices (Kp, Dst) during September 6–10, 2017. These two subfigures can be obtained from the PPSWAP App, developed by SEPC of NNSC (http://www.sepc.ac.cn). As can be seen from Fig. 2, during September 8th, the geomagnetism reached the level of a large magnetic storm (Kp = 7 or 8) in 12 h, medium magnetic storm (Kp = 6) in 3 h, and small magnetic storm (Kp = 5) in 9 h. The geomagnetic index Dst in Fig. 2 showed a corresponding variation to that of Kp. With the development of the magnetic storm, the Dst index reached the first minimum value of – 144 nT at 1 UTC and the second minimum value of – 124 nT at 17 UTC on Sept 08, which indicates the X9.3 solar flare on September 6 triggered a double main phase sudden commencement magnetic storm. To analyze the ionospheric response to the magnetic storm, the global ionosphere maps (GIMs) with a 2-h resolution from Sept 07 UTC00:00 to Sept 09 UTC 22:00 in 2017 are drawn using the vertical TEC data provided by IGS station, as shown in Fig. 3. First of all, from the time response of TEC to the magnetic storm, and comparing Kp and Dst index, it is obvious that with the occurrence of the magnetic storm, TEC increased slowly during the early stage of Sept 07, 2017. Then, it increased significantly since 18: 00 on Sept 7, 2017, reaching the first maximum on Sept 08 UTC 02:00. After that, it descended and remained stable between 06: 00 and 14: 00. It began to rise again at 16: 00 and reached the second maximum at 22: 00 on Sept 08. During the period of 9 September, it gradually recovered to a stable state.

The two maximum values of TEC corresponded to the two minimum values of Dst, and its change trend is generally consistent with the Dst and Kp indices. However, during the second main phase, the TEC maximum has a time delay relative to the Dst minimum. In addition, observing each map in combination with the UTC in Fig. 3, it can be seen that TEC has a significant diurnal variation, reaching the maximum value around 14:00 local time. This is because the solar radiation is strongest at noon, which enhances the ionization of atmospheric molecules; therefore, the electron concentration gradually increases until reaching its maximum in about two hours. According to the spatial distribution of TEC, the magnetic storm has the greatest impact on low latitudes, especially the enhancement near 20° north–south latitude. The white dotted line in the figure represents the magnetic equator. In the period around the two maxima, the equatorial bimodal structure symmetrical about the magnetic equator appeared, which is also called an equatorial anomaly.

Fig. 1 Example of disturbed electron density and TEC profiles from COSMIC (blue lines in **a, c,** respectively). The red lines in **a, c** denote the electron density and TEC data smoothed by five-point moving average method, respectively. **b, d** The electron density and TEC fluctuations filtered by five-point moving average method, respectively. The study is focused on the region *of F*2 peak height $h = 300$–350 km (color figure online)
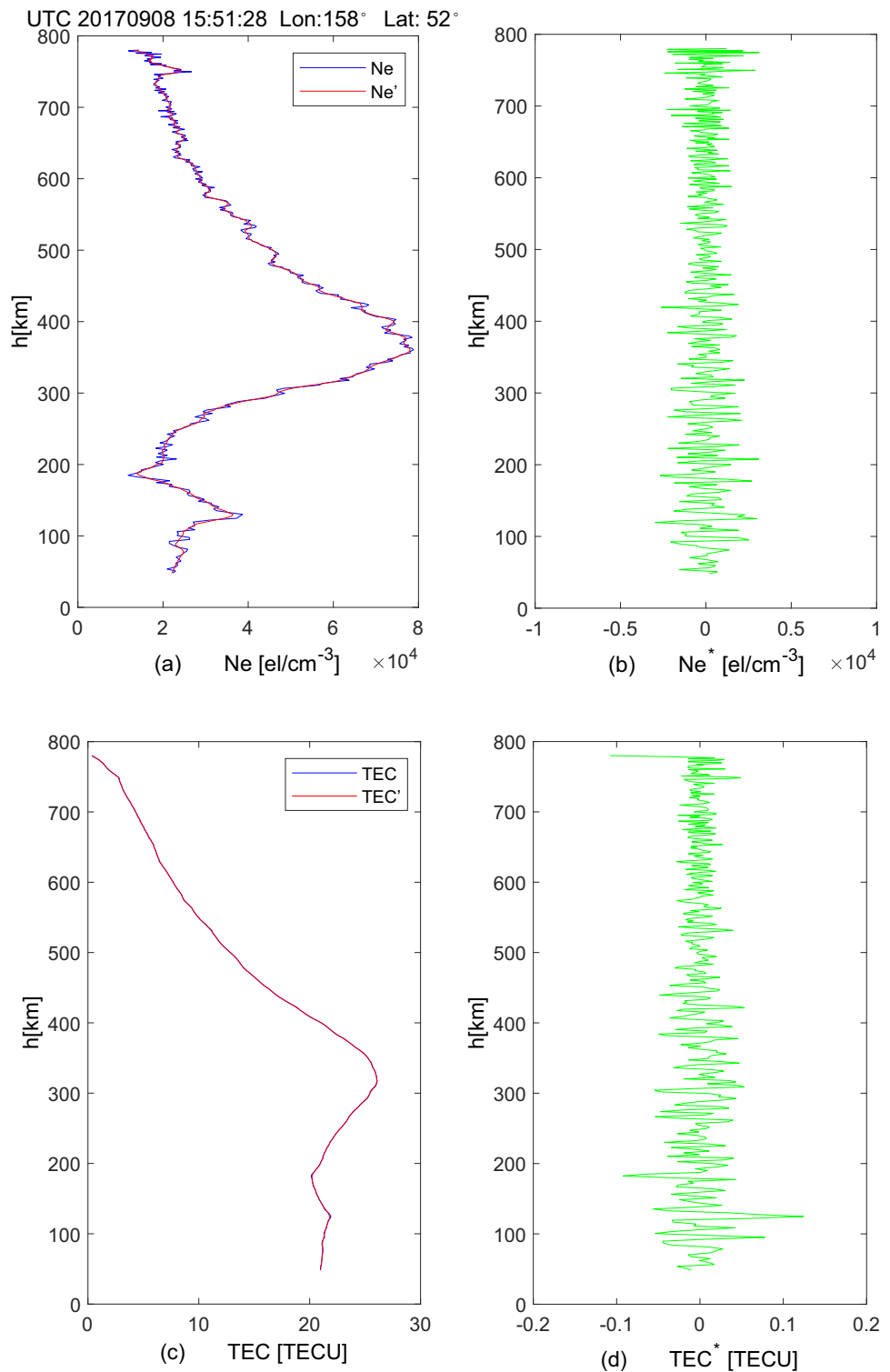

3.2 Result based on space-based data

The global maps of ΔNe and ΔTEC are plotted in Fig. 4a, b, respectively. They are all selected on September 8, 2017, with tangent points at $h = 300$–350 km (around F2 peak height). In

this paper, we adopt the percentage standard for ΔNe and the RMS standard for ΔTEC. Due to the aging and loss of the satellites, the number of occultation events is insufficient. In this study, the grids without data are all mapped to the minimum value on the color bar (dark blue). Although we

Fig. 2 Variations of Kp and Dst indices during September 6–10, 2017
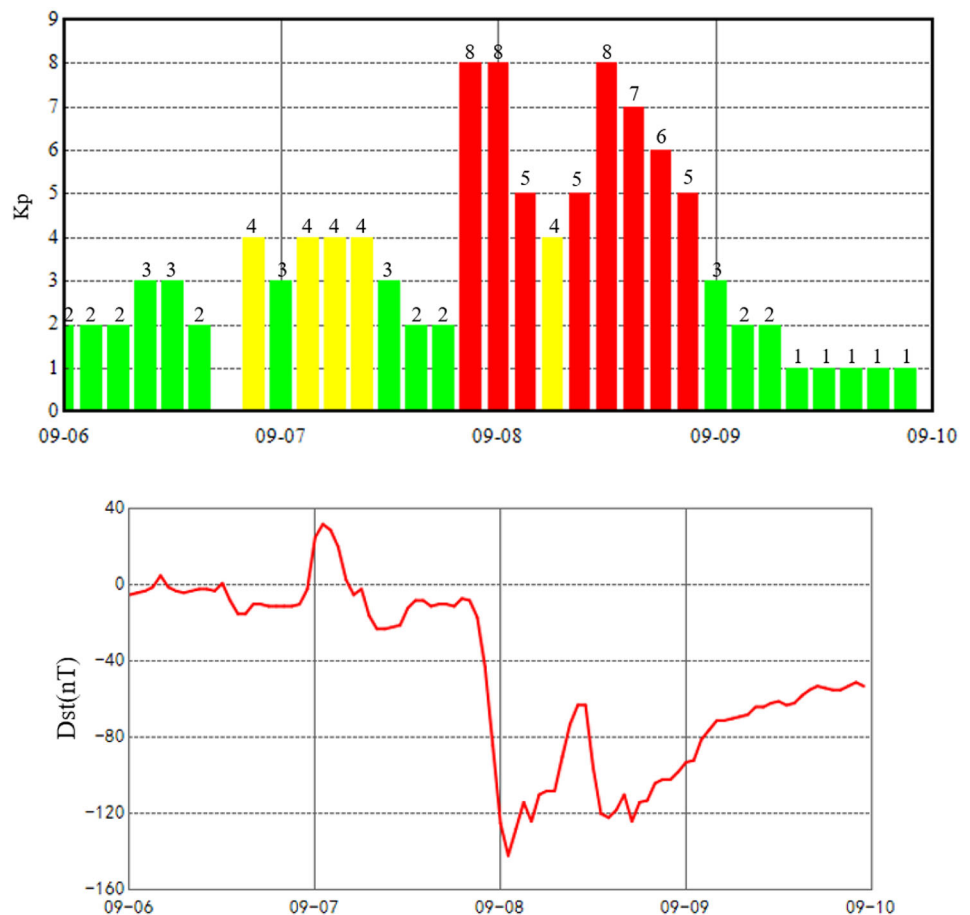
have removed the unreasonable profiles, there are still some outliers due to observation errors and approximation errors. For the larger outliers, we map them to the maximum value on the color bar (dark red) as well.

As we can see in Fig. 4a, b, these two maps show different disturbance distributions. For ΔNe, there are obvious fluctuations in the middle and high latitudes, while for ΔTEC, there are large fluctuations in middle and low latitudes, especially in the Atlantic Ocean, which may result from the sporadic appearance of equatorial plasma bubbles in F2 region. The reason may be that the Ne profile mainly characterizes the vertical direction of the ionosphere, while TEC characterizes the horizontal direction of the ionosphere along the LEO-GPS ray paths in each RO event.

When the radio wave passes through the ionosphere, it is usually affected by the irregularities in the ionosphere, resulting in fluctuations of signal amplitude and phase. Therefore, the ionospheric scintillation can also reflect the disturbance of the ionospheric irregularities. As a supplement, we also plot the global distribution of ionospheric scintillation index S4 on September 8, 2017, as shown in Fig. 4c. $S4$ is the magnitude of signal amplitude fluctuation, and $0.2 < S4 < 0.4$ indicates weak scintillation, $0.4 < S4 < 0.6$ indicates moder-

ate scintillation, and $S4 > 0.6$ indicates strong scintillation. As can be seen from Fig. 4c, weak scintillation occurred in most parts of the world on September 8, 2017. Moderate scintillation is mainly concentrated around 120 ° W and 100 ° E, which is consistent with the distribution of ΔNe. However, all these three maps show the asymmetry between the north and the south, and the disturbance in the southern hemisphere is slightly larger. This north–south asymmetry is possibly caused by the positive deviations of the BX and BY components of the interplanetary magnetic field [8].

4 Summary

In this study, we took one of the magnetic storm events occurred in September 2017 to investigate the spatial–temporal responses of the ionosphere disturbances during the magnetic storm.

First, the geomagnetic data and IGS vertical Total Electron Content (TEC) data were used to analyze the temporal and spatial distribution changes of TEC during the geomagnetic storm. We found that the TEC shows a corresponding variation and a negative correlation with the Kp and Dst index,

Fig. 3 Global ionosphere TEC (TECU) map during Sept 07–09, 2017, with a 2-h time resolution
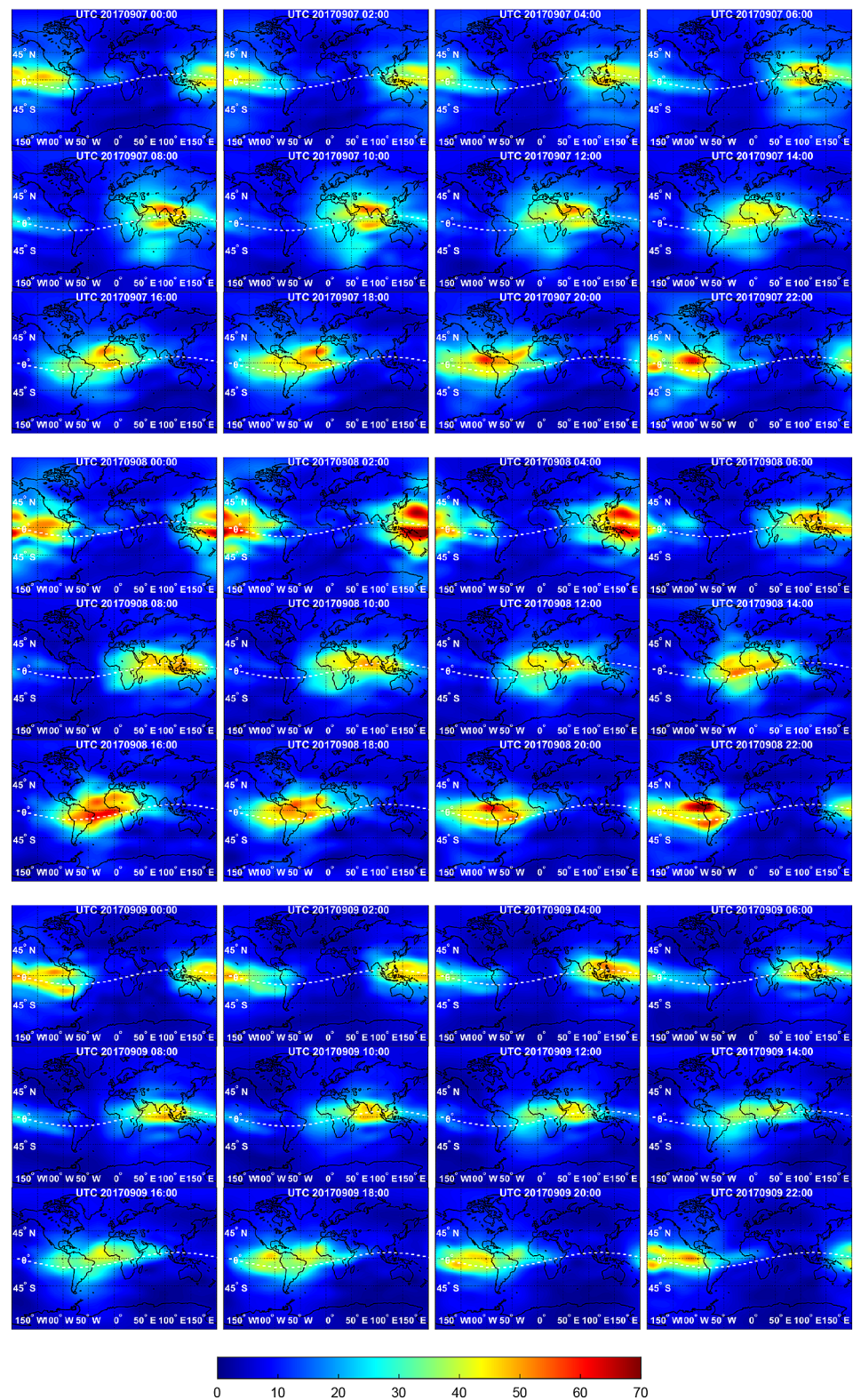

respectively, which characterize the intensity of geomagnetic disturbance. And it has a significant diurnal variation, reaching the maximum value around 14:00 local time because of solar radiation. From the spatial response, we find significant TEC enhancement occurs in low latitudes, increasing most obviously in the equatorial anomaly area.

Then, the spatial fluctuations based on post-processed electron density and total electron content from COSMIC and

Fig. 4 a Global map of ΔNe (with tangent points at $h = 300$–350 km) on September 8, 2017, adopting the standard of percentage, fusing COSMIC and GRACE satellite data. **b** Global map of ΔTEC (with tangent points at $h = 300$–350 km) on September 8, 2017, adopting the standard of RMS, fusing COSMIC and GRACE satellite data. **c** Global map of S4 on September 8, 2017, based on COSMIC observation (color figure online)
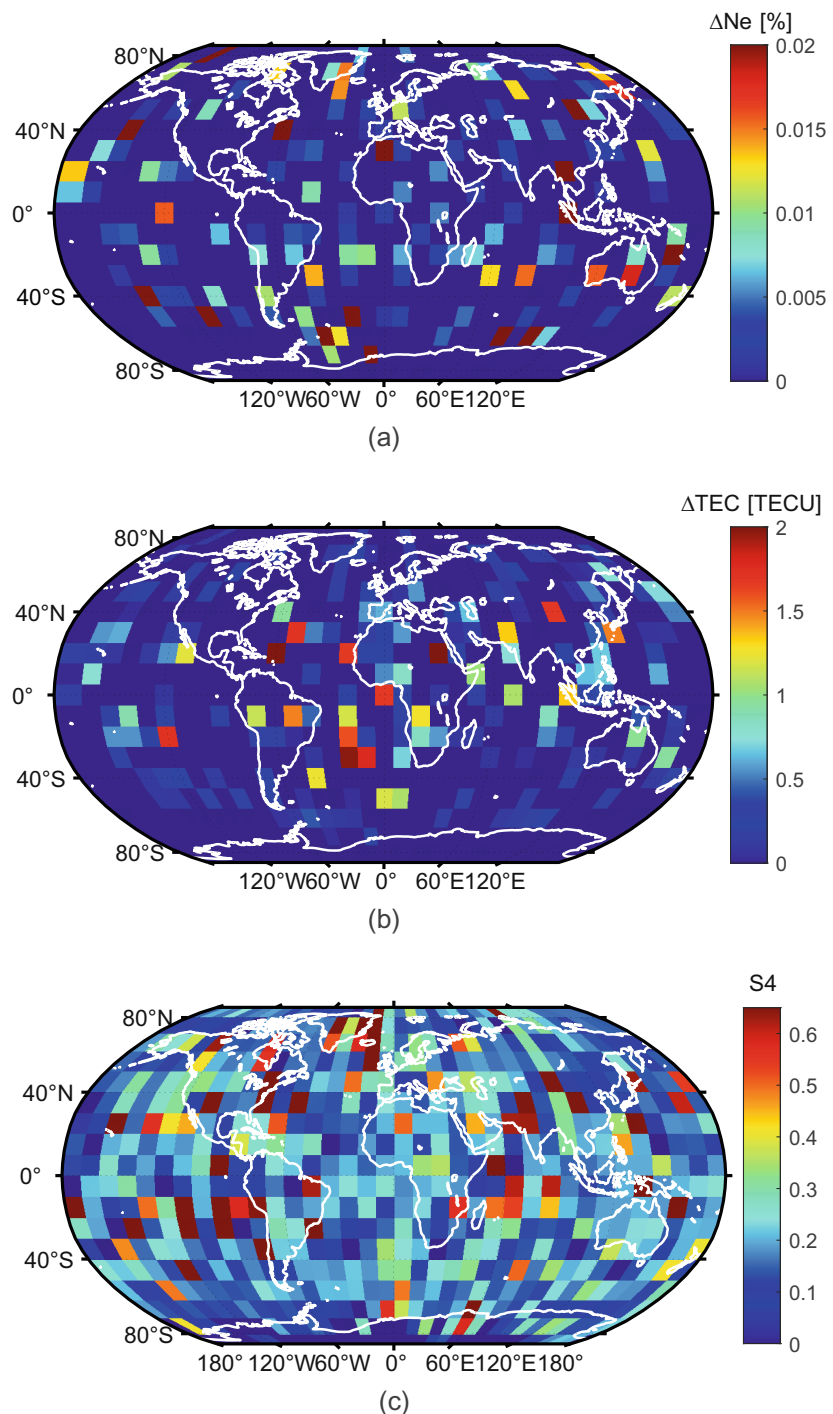
GRACE missions were extracted using a five-point moving average method. The percentage of electron density fluctuations (ΔNe) and the RMS of TEC fluctuations(ΔTEC) were calculated. And the global maps of electron density and TEC fluctuations on September 8, 2017, with tangent points at $h = 300$–350 km, were given. We found that they show different characteristics in spatial distribution. For ΔNe, there are obvious fluctuations in the middle and high latitudes, while

for ΔTEC, there are large fluctuations in middle and low latitudes, which may be caused by the horizontal and vertical gradient differences of plasma around F2 peak height.

Finally, we plotted the global distribution of ionospheric scintillation index S4 on September 8, 2017. Results show that weak scintillation occurred in most parts of the world on September 8, 2017, while moderate scintillation is mainly concentrated around 120° W and 100° E, similar to the dis-

tribution of electron density fluctuations. And all these three maps show the asymmetry between the north and the south, and the disturbance in the southern hemisphere is larger.

The spatial–temporal sampling of the ionosphere by only one LEO satellites of the COSMIC mission is insufficient for a case study of a geomagnetic storm. However, this paper can provide a better understanding of the global ionosphere disturbance driven by space weather events and can also facilitate the detection and mitigation of ionosphere scintillations on a space-based platform. In the future, we will assimilate more data sources to have an in-depth investigation on the ionospheric disturbances during this geomagnetic storm event. In addition, the novel COSMIC-2 has been successfully launched at UTC07:30 on June 25, 2019. There will be better findings with sufficient data. We will conduct more analysis on ionosphere disturbances and GNSS scintillation events with sufficient data sets in the future.

References

1. Mendillo M (2006) Storms in the ionosphere: patterns and processes for total electron content. Rev Geophys 44(4):1–41
2. Lin K, Zhan X, Huang J (2019) GNSS signals ionospheric propagation characteristics in space service volume. Int J Sp Sci Eng 5(3):223–241
3. Yasyukevich Y, Astafyeva E, Padokhin A, Ivanova V, Syrovatskii S, Podlesnyi A (2018) The 6 September 2017 X-class solar flares and their impacts on the ionosphere, GNSS, and HF radio wave propagation. Sp Weather 16(8):1013–1027
4. Yang R., Xu D, Morton Y T (2019) Generalized multi-frequency GPS carrier tracking architecture: design and performance analysis. IEEE Trans Aerosp Electron Syst 56(4):2548–2563
5. Yang Z (2018) Investigation of equatorial ionosphere scintillations using GNSS observations from Hong Kong region
6. Berdermann J, Kriegel M, Banyś D, Heymann F, Hoque MM, Wilken V, Jakowski N (2018) Ionospheric response to the X9. 3 Flare on 6 September 2017 and its implication for navigation services over Europe. Sp Weather 16(10):1604–1615
7. Lei J, Huang F, Chen X, Zhong J, Ren D, Wang W, Hu L (2018) Was magnetic storm the only driver of the long-duration enhancements of daytime total electron content in the Asian–Australian sector between 7 and 12 September 2017. J Geophys Res Sp Phys 123(4):3217–3232
8. Hocke K, Liu H, Pedatella N, Ma G (2019) Global sounding of F region irregularities by COSMIC during a geomagnetic storm. Ann Geophys 37(2):235–242
9. Yeh WH, Lin CY, Liu JY, Chen SP, HsiaoT Y, Huang CY (2019) Superposition property of the ionospheric scintillation S4 index. IEEE Geosci Remote Sens Lett 17(4):597–600
10. Yang R, Zhan X, Huang J (2020) Robust GNSS triple-carrier joint estimations under strong ionosphere scintillation. China satellite navigation conference. Springer, Singapore, pp 562–575
11. Li W, Huang L, Zhang S, Chai Y (2019) Assessing global ionosphere TEC maps with satellite altimetry and ionospheric radio occultation observations. Sensors 19(24):5489
12. Zakharenkova IE, Krankowski A, Shagimuratov II, Cherniak YV, Krypiak-Gregorczyk A, Wielgosz P, Lagovsky AF (2012) Observation of the ionospheric storm of October 11, 2008 using FORMOSAT-3/COSMIC data. Earth Planets Sp 64(6):505–512
13. Tsai LC, Su SY, Liu CH, Schuh H, Wickert J, Alizadeh MM (2018) Global morphology of ionospheric sporadic E layer from the FormoSat-3/COSMIC GPS radio occultation experiment. GPS Solut 22(4):118
14. Rocken C, Ying-Hwa K, Schreiner WS, Hunt D, Sokolovskiy S, McCormick C (2000) COSMIC system description. Terres Atmos Ocean Sci 11(1):21–52
15. Anthes RA, Bernhardt PA, Chen Y, Cucurull L, Dymond KF, Ector D, Liu H (2008) The COSMIC/FORMOSAT-3 mission: early results. Bull Am Meteor Soc 89(3):313–334
16. Wang H, Luo J, Xu X (2019) Ionospheric peak parameters retrieved from FY-3C radio occultation: a statistical comparison with measurements from COSMIC RO and digisondes over the globe. Remote Sens 11(12):1419
17. Wickert J, Beyerle G, König R, Heise S, Grunwaldt L, Michalak G, Schmidt T (2005) GPS radio occultation with CHAMP and GRACE: a first look at a new and promising satellite configuration for global atmospheric sounding. Ann Geophys 23(3):653–658
18. Lei J, Syndergaard S, Burns AG, Solomon SC, Wang W, Zeng Z, Zhang SR (2007) Comparison of COSMIC ionospheric measurements with ground-based observations and model predictions: preliminary results. J Geophys Res Sp Phys 112(A7):A07308. https://doi.org/10.1029/2006JA012240
19. Kuo YH, Wee TK, Sokolovskiy S, Rocken C, Schreiner W, Hunt D, Anthes RA (2004) Inversion and error estimation of GPS radio occultation data. J Meteorol Soc Jpn Ser II 82(1B):507–531
20. Syndergaard S, Schreiner WS, Rocken C, Hunt DC, Dymond KF (2006) Preparing for COSMIC: Inversion and analysis of ionospheric data products. Atmosphere and climate. Springer, Berlin, pp 137–146
21. Wang Q, Fang H, Niu J (2016) Analysis of ionospheric irregularities in f layer based on cosmic data. Geophys J 059(002):419–425
22. Yang KF, Chu YH, Su CL, Ko HT, Wang CY (2009) An examination of FORMOSAT-3/COSMIC ionospheric electron density profile: data quality criteria and comparisons with the IRI model. Terres Atmos Ocean Sci 20(1):193
23. Li C (2011) COSMIC electron density data analysis. Dissertation, Guilin University of Electronic Technology
24. Sun F, Luo J, Xu X, Wang H (2020) Comparisons of ionospheric peak parameters from radio occultation observations and IRI-2016 model outputs over China. Geomat Inform Sci Wuhan Univ 45(3):403–410. https://doi.org/10.13203/j.whugis20180391